Thermophysics and Aeromechanics, *2021*, *Vol. 28*, *No. 3*

DOI: 10.1134/S0869864321030045

Numerical simulation of turbulent flow around a 3D hydrofoil under the effect of corner separation*

A.V. Sentyabov[1,2], A.A. Gavrilov[1,2], and A.A. Dekterev[1,2]

[1]*Kutateladze Institute of Thermophysics SB RAS*, *Novosibirsk*, *Russia*

[2]*Siberian Federal University*, *Krasnoyarsk*, *Russia*

E-mail: sentyabov_a_v@mail.ru

(*Received November 22*, *2020*; *revised February 20*, *2021*;
accepted for publication March 23, *2021*)

The paper presents the results of numerical simulation of three-dimensional turbulent flow around a hydraulic turbine guide vane at the angle of attack of 9º with the aspect ratio of the foil equal to 0.8. The influence of turbulence modeling variants on 3D flow effects is analyzed. The 3D boundary layer separation at the vane-sidewall junctions and the flow separation near the trailing edge influence the flow pattern. The study considered various approaches for modeling of a turbulent flow, such as the k-ω SST turbulent viscosity model and several variants of the differential and algebraic Reynolds stress models. At the given angle of attack, the k-ω SST model shows a significant separation zone in the corners between the wall and the vane, while no separation of the flow in the central plane is observed. Both differential and algebraic Reynolds stress models reproduce the secondary vortex flow at the corners and suppress the flow separation near the central cross section.

Keywords: hydrofoil, numerical modeling, turbulence, RSM.

Introduction

Unlike the fluid mechanics in hydropower equipment, the foil profiles have the across dimensions compared to the foil chord length. A typical example is a guide vane of the hydroturbine. The vane's quasi-2D shape is fitted to a limited space between the turbine chamber walls. The analogous situation is observed for the impeller vanes. Here the corner effects might have a significant contribution to the turbulent flow past the hydrofoils (especially with the phenomena of separation or cavitation). However, the turbulence models (based on the turbulent viscosity hypothesis) are fitted mainly to simulation of 2D boundary layers and incapable to reproduce such effect as the secondary vortex flow in corners: this kind of simulation requires the Reynolds stress models.

The secondary vortex flow developing due to anisotropic turbulent effects was discovered for the channels of rectangular shape. Nikuradze [1] found in 1926 that the isolines of the axial component of velocity in a direct duct (with a rectangular cross section) are shifted

* The research was funded by RFBR, Krasnoyarsk Territory and Krasnoyarsk Regional Fund of Science, project number 20-41-240004. Development of the computational model was supported by the Ministry of Science and Higher Education of the Russian Federation (project No. AAAA-121031800229-1).

towards the corners of the duct. Flow visualization using a dye tracer demonstrated a pattern of secondary eddy flow induced in the mainstream-normal plane: this vortex pushes the fluid with a high longitudinal momentum towards the duct corners from the center. The paper [2] demonstrated that the vortex generation occurs due to a gradient of normal components of the Reynolds stress tensor. However, the models of linear eddy viscosity assume that the normal turbulent stresses are isotropic: thus, those models cannot reproduce this effect. Another paper [3] illustrates the role of gradients of turbulent shear stress in inducing a secondary flow in the rectangular channel. A theoretical study [4] of the secondary flow induced by skew and stress used the equations for the average vorticity. The shortcomings of the linear turbulent viscosity models for simulation of the flow in a rectangular-section duct were explained in [5] (the authors used the nonlinear models k-ε and k-l). This model was used for the simulation of flow in a duct and found generation of 8 vortices in the duct cross section. Paper [6] presented an investigation of a turbulent flow in a squared duct; the authors used a model with closure of second order and elliptic-type relaxation in the near-wall layer. It was concluded that the second-order closure models tend to underestimate the intensity of a secondary flow in a non-round channel, but the near-wall functions cannot reproduce the main flow mechanisms. The study [7] uses the model of the Reynolds stress transfer for modeling of a steady or a rotating rectangular duct with the aspect ratio equal to 4. The authors noted a significant influence of the secondary vortices on the wall shear stress distribution (even at the background of low intensity). It was demonstrated that the second order closure models can reproduce these vortices and have a good compliance with experimental data. A research of turbulent flow in channels with different geometries was presented in [8] and [9] using the RSM and DNS models. The study [8] demonstrated a role of turbulent pulsation anisotropy in a rectangular channel. This means an advantage of the second-order model as compared to the linear eddy-viscosity model. Paper [9] compared the flows in channels with different shapes (circular, squared, and with wall corrugations). The authors found that the corrugation (and in corners of a rectangular duct) creates a return flow directed from the channel center towards the corrugations. Numerical experiments [10] demonstrated a big role of a weak secondary flow in the rectangular channel on the flow detachment in the downstream diffuser.

The improper modeling for the secondary flow produces errors in simulation of flow over a 3D airfoil. For example, publication [11] presents a v2f model for improving the simulation for a 3D boundary layer in the wing-fuselage junction zone. The linear and nonlinear models of eddy-viscosity and the differential model of Reynolds stress transfer were used [12] for the study of a turbulent flow over the NACA0020 wing installed on a flat sheet. The closure models of second order have several advantages for simulation of the U-shaped vortex. Paper [13] was devoted to flow simulation over a test model of DLR F-6 aircraft (shown in [14]): it was found that the k-ω SST model overestimates the size of detachment zone in the wing-fuselage junction zone. The same kind of test was used in [15] for validation of the algebraic model of Reynolds stress transfer BSL-EARSM, which demonstrated a more correct description of in-corner flow detachment. This study also estimates the effect of anisotropy of the diagonal Reynolds stress: it was compared with computations using only the isotropic part of the developed BSL-EARSM model. Here the isotropic version of model slightly reduces the separation region inside the corner (compared to k-ω SST model), but the bigger improvement of results was achieved due to the anisotropic model.

For the conditions of a long wing, the error in corner detachment modeling is insignificant for estimation of the lifting force and drag. The situation with modeling in hydropower engines can be different: the foil profiles usually have similar longitudinal and transversal dimensions. The study [16] deals with cavitation-load and cavitation-free flow past a vane of the hydroturbine wicket gate: the authors noticed for the attack angle of 9º and cavitation-free flow a high difference between the simulated velocity profiles and experimental data. Although the PIV measurements revealed the flow detachment in the central plane, the 3D simulation with k-ω SST model (or a developed DDES model) demonstrated the separation-free flow. Meanwhile, the 3D effects are significant for study of cavitation flow for the studied vane.

The experimental study [17] for this vane with the attack angle of 9º had found the cavitation instability which develops along the wing span. Besides, the 3D simulation is a must for study of cavitation in a flow through the end clearance between the vane and the walls [18].

In paper [17], the significance of the turbulence simulation for 3D flow around the hydroturbine flow duct of the turbine wicket gate was estimated through numerical study of cavitation-free flow past a vane of wicket gate and comparison with experimental data [17]. Experiments provided the velocity profiles on the suction side of vane: this allows one to estimate the corner effects, in particular, on the flow separation in the foil middle zone.

1. Numerical model

The study was performed for the scale model of a vane in a wicket gate of a high-head hydropower station (with the main chord length C = 100 mm). The simulation domain is part of the duct of a hydraulic test bench. The experimental procedure for this setup was described in works [17, 19, 20]. This zone comprises the inlet confusor and the working channel with a mounted hydrofoil (Fig. 1). The hydrofoil axis was in the middle of the working section's height equal 2.5C, while the hydrofoil width was 0.8C, which coincides with the working section width.

Distilled water was taken as working fluid. The parameters of the medium (according to experimental data) were taken at the temperature of 30 °C (Table 1). The input mass flow rate was 161.4 kg/s. The mass flow rate was calculated from experiments as a product of the average velocity, water density for the known conditions, and the duct cross-section area. The flow velocity in the working duct U_0 was 8.1 m/s and it was evaluated from PIV measurements at a certain shift upstream of the foil.

Computations were performed using the Ansys Fluent 17.1 soft package and the control volume method. Turbulence modeling was performed using the models of different levels: the k-ω SST model based on the eddy-viscosity approximation [21], differential Reynolds stress model (two modifications), and the algebraic Reynolds stress model. As for the differential Reynolds stress model, we chose the versions using the equations for specific dissipation rate ω: this allows one to resolve the boundary layer from the wall. The first version of ω-based RSM model (RSM-ω, [22]) uses the equation for ω taken from the k-ω model. The second version (RSM-BSL) takes the equation

Table 1

Working fluid properties at the temperature 30 °C (for distilled water)

ρ, kg/m^3	996
μ, Pa·s	$0.79 \cdot 10^{-3}$

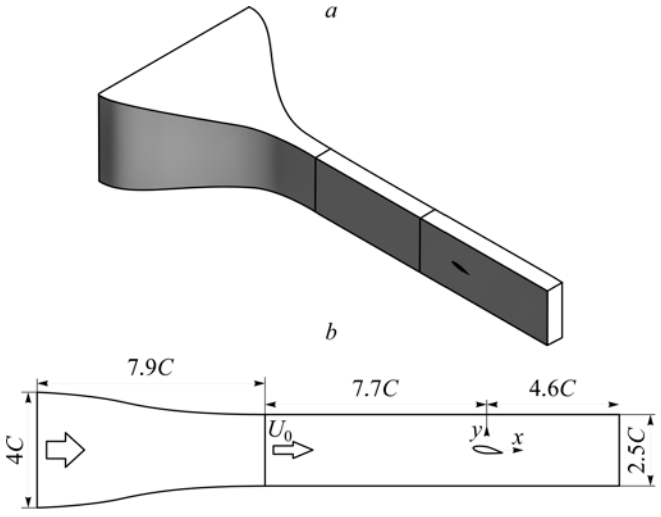

Fig. 1. Simulation domain in 3D shape (*a*) and the diagram (*b*).

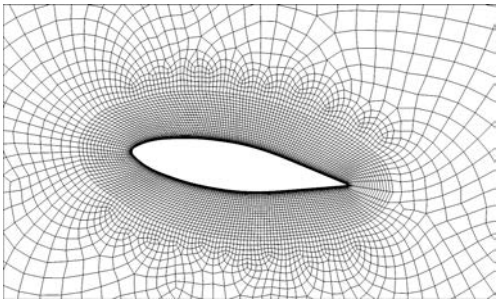

Fig. 2. CFD grid.

Table 2

CFD grid parameters

No.	Number of cell, thsnds.	y_+ at the sidewall
1	224	< 350
2	317	< 250
3	317	<120
4	1160	< 10

for ω from the k-ω BSL model (baseline). The second version of equation for ω is the best for eliminating the undesired sensitivity for the freestream conditions (typical of Wilcox's model).

The linear model LRR [23] is used in both cases for calculation of the redistribution term in the Reynolds stress equations. The presented version of explicit algebraic model for Reynolds stress (BSL-EARSM) is a combination of BSL model and Wallin–Johansson relation for stress [15]. It was shown in [15] that this model is suitable for calculation of in-corner separation flow in the zone of wing-fuselage junction.

The simulation was based on 3D simulation grids comprised from hexahedral cells. In the hydrofoil vicinity, we take a near wall layer with condensed coordinate lines towards the foil surface. The rest of domain is covered by more sparse unstructured grid (Fig. 2). On the average, the dimensionless distance from the foil wall up to the first node of computations was about $y_+ \sim 1$, i.e., the boundary layer can be resolved from the wall. In the wingspan direction, the grid was condensed near the sidewalls with a different level of resolution, up to $y_+ < 10$ for the basic grid. The basic grid comprises about 1100 thousands of control volumes. The other versions were different in the spanwise direction resolution, and the grid characteristics are presented in Table 2.

The velocity-pressure link during computations was provided with SIMPLEC algorithm (see [24] and [25]). The convection terms in the momentum transfer equation were approximated by a central-difference scheme [26], while the equations of turbulence transfer were described by a first-order upwind scheme.

2. Results

Comparison of simulation with experimental data demonstrates that the 2D simulation using the k-ω SST model is proper for describing the flow past a wing profile, including the case of flow separation from the trailing edge (Fig. 3). This figure presents the graphs of the longitudinal component of velocity for different cross sections in the central streamwise

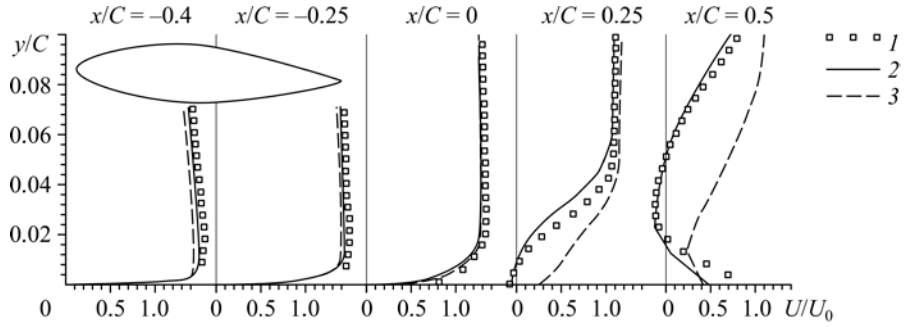

Fig. 3. Velocity profiles compared.
Experimental data (*1*) and results of 2D (*2*) and 3D (*3*) simulations by k-ω SST model.

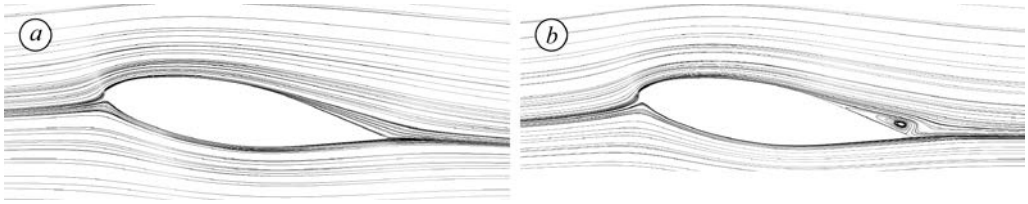

Fig. 4. Streamlines in the central cross section.
Results of 3D simulation on the grid No. 4 using *k*-*ω* SST model (*a*) and RSM-BSL model (*b*).

plane (a symmetry plane) taken at the suction face. The vertical axis is a plot of the distance to the foil wall along the O*y* axis, and the horizontal axis is the velocity normalized by the superficial velocity through the passage cross section — U_0 = 8.1 m/s. Since the Reynolds number is rather high, the boundary layer thickness is extremely low, so data is presented for a thin layer near the vane surface. Although the 2D simulation demonstrates good results, we have to take into account 3D effects for this geometry [17]. Meanwhile, the 3D simulation produces a worse matching to experimental data, even for a fine mesh No. 4. For both cases (2D and 3D), the calculated velocity profiles are similar to experimental curves above the first half of the vane — from the front edge up to the separation point: the good compliance occurs for the zone of potential flow and for the boundary layer. However, the experimental data reveal a flow separation near the rear edge at the coordinate $x/C \approx 0.75$, but the 3D simulation (performed with *k*-*ω* SST model) demonstrates almost separation-free flow, as shown in Fig. 4*a*. On the opposite, the 2D simulation (using the same model) demonstrates flow separation at the rear edge and the velocity profiles on the suction face are close to experiment (before and after separation of the boundary layer).

The reason for discrepancy between 3D simulation and 2D simulation along with experimental data is a broad corner separation at the sidewalls of the working duct (Fig. 5*a*). The recirculation zone (induced by the lateral separation) occupies almost the entire zone above the vane in the diffuser part of flow. This phenomenon squeezes the flow in the central plane and this prevents the flow separation here. This kind of results is typical of the turbulence models based on the linear eddy viscosity. Since the listed models of turbulent viscosity are inadequate for corner separation (they overestimate separation), we performed this kind of flow using

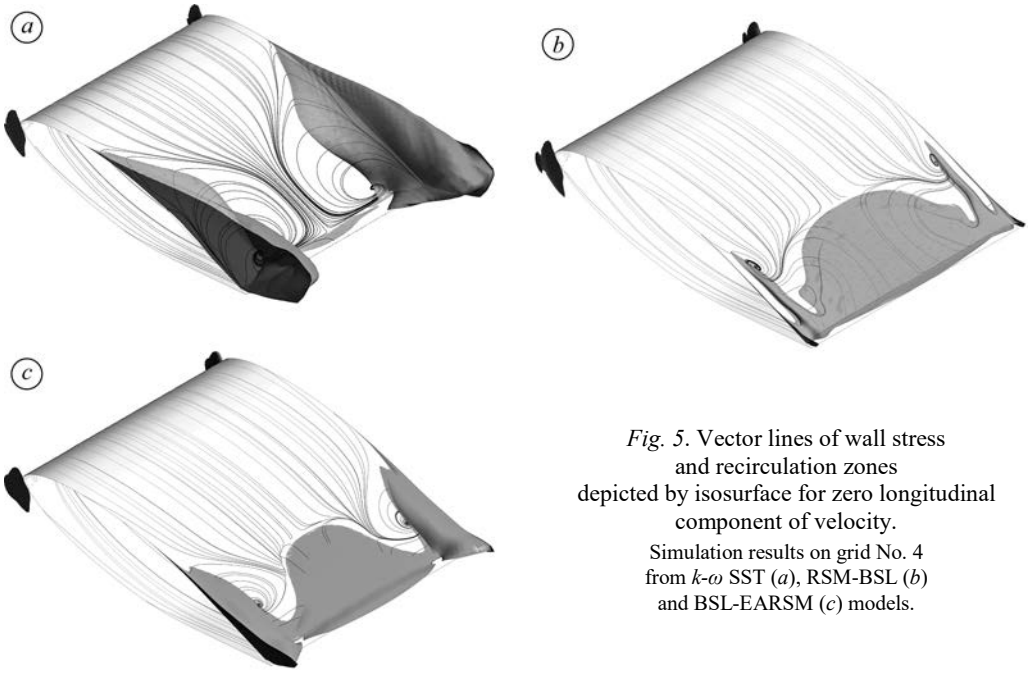

Fig. 5. Vector lines of wall stress and recirculation zones depicted by isosurface for zero longitudinal component of velocity.
Simulation results on grid No. 4 from *k*-*ω* SST (*a*), RSM-BSL (*b*) and BSL-EARSM (*c*) models.

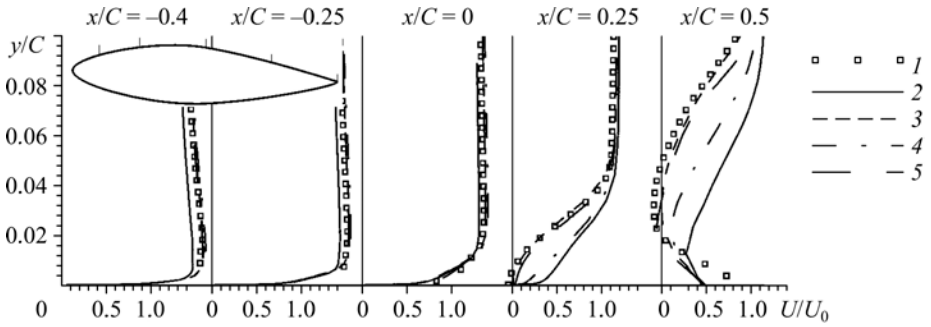

Fig. 6. Comparison of velocity profiles calculated using different models of turbulence for refined computation on grid No. 4. Results of experiment (*1*) and computations using *k*-*ω* SST (*1*), RSM-BSL (*2*), RSM-*ω* (*3*), and EARSM (*4*) model.

the Reynolds stress models (RSM). Calculation with the RSM-BSL model revealed the flow separation in the central plane (Fig. 4*b*) at lower values of corner separation (compared to *k*-*ω* SST models) – see Fig. 5. The algebraic Reynolds stress model (BSL-EARSM) demonstrates similar results – see Fig. 5*c*.

Comparison of velocity profiles in the central plane demonstrates that the simulation by RSM-BSL model is in compliance with experimental data and depicts the flow separation at the rear edge properly (Fig. 6). We should note that the results from the *ω*-based RSM model are closer to experimental data than the alternative *k*-*ω* SST model. At that, the results from the BSL-EARSM model are very close to the corresponding differential model RSM BSL.

The results in the flow structure are critical for the vane-acting forces. Table 3 presents the linear coefficients for drag and for lifting force which are calculated by formula $C_l = F/(\rho U_0^2 Cl/2)$, where F is the lift force, and l is the vane length in z direction. One can see that the lift force calculated by *k*-*ω* SST model is twice lower and the drag force is by 1.6 times higher than for RSM model. Both versions of differential model of RSM and algebraic RSM model produce similar results.

The computation grid refining in the span direction is significant for simulation results. This was confirmed by computations on several meshes (see parameters in Table 2). In general, better refining of the boundary layer at the sidewalls produces a better simulation for the separation flow (Fig. 7). However, the results for the grid No. 3 (coarse but refined towards the sidewalls) is very close to that for fine grid No. 4.

The reason why the Reynolds stress model is more accurate in reproducing the corner separation phenomenon is, obviously, due to the secondary flows in the corners (the result of turbulence pulsation anisotropy [15]). According to the results from [2] and [5], the longitudinal component of vorticity in the corner of a rectangular channel is generated due to the anisotropy of the Reynolds stress tensor in the plane normal to the flow:

$$\left(U_y\frac{\partial\Omega_x}{\partial y}+U_z\frac{\partial\Omega_x}{\partial z}\right)=\frac{\partial^2}{\partial y\partial z}\left(\overline{u_z^2}-\overline{u_y^2}\right)-\left(\frac{\partial^2}{\partial y^2}-\frac{\partial^2}{\partial z^2}\right)\overline{u_y u_z}+\nu\left(\frac{\partial^2}{\partial y^2}+\frac{\partial^2}{\partial z^2}\right)\Omega_x,$$

where **U** is the velocity vector, Ω_x is the longitudinal component of vorticity vector, **u** is the velocity pulsation, and ν is the viscosity. This equation illustrates that the turbulent flow produces the longitudinal vorticity due to existence of the gradient in the Reynolds stress tensor components.

Table 3

Drag and lifting force coefficients

Model	C_x	C_y
k-*ω* SST	0.074	0.35
RSM BSL	0.046	0.74
RSM *ω*-based	0.045	0.82
BSL-EARSM	0.047	0.68

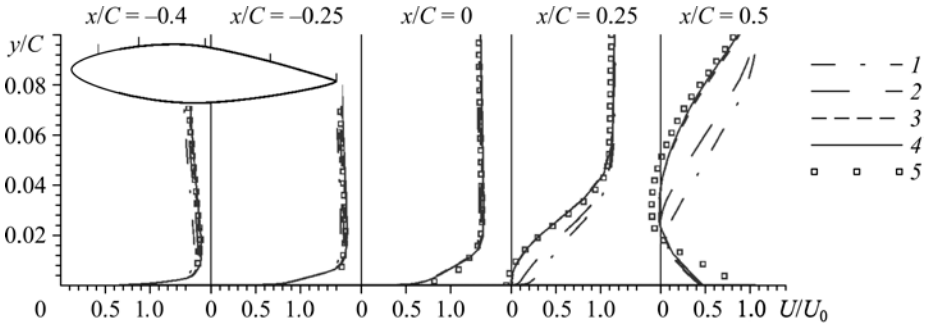

Fig. 7. Comparison of velocity profiles in the central plane, produced on different meshes using the RSM-BSL model.
Digits *1–4* correspond to numbers from Table 2, *5* — experimental data.

Figure 8 demonstrates existence of explicit anisotropy of turbulence in the corner between the vane and the butt wall. The Reynolds stress model creates the recirculation flow in the *y*O*z* plane: it captures the mainstream to the corner and this increases the longitudinal

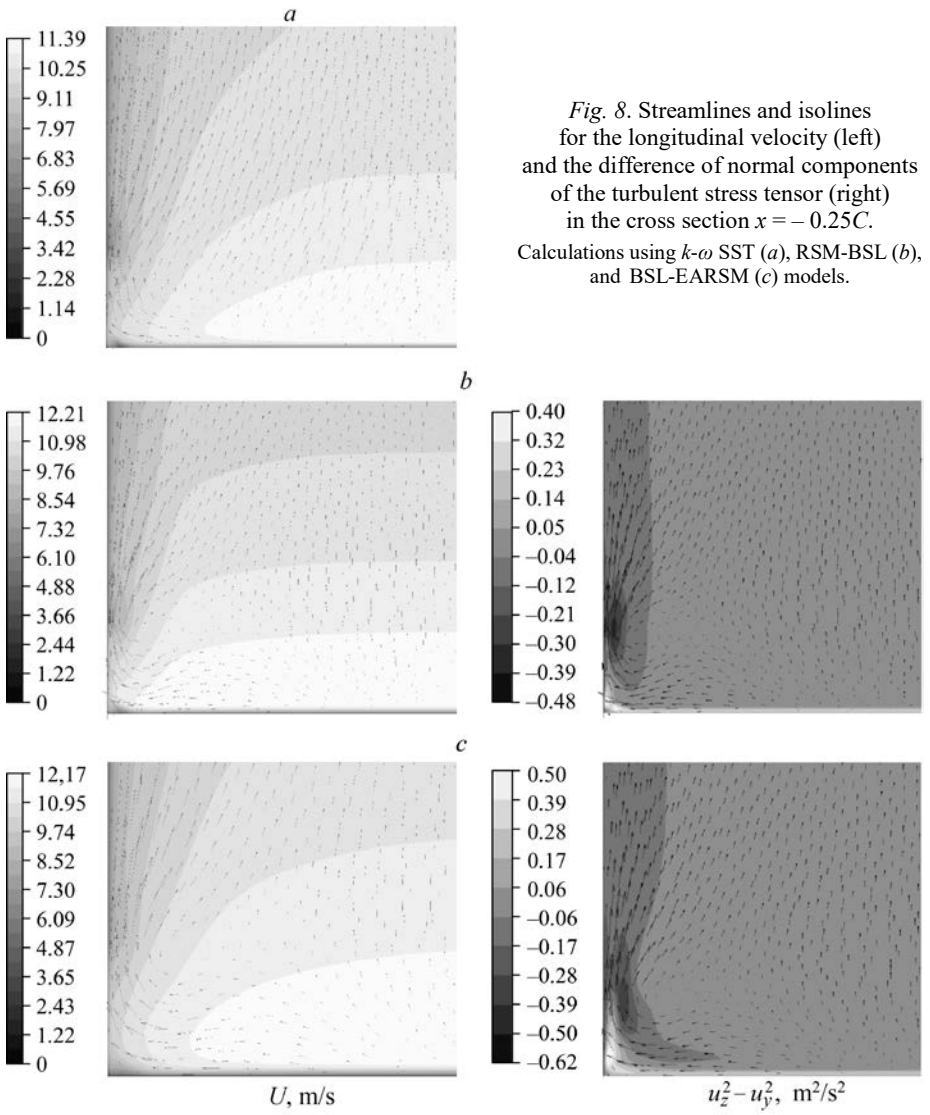

Fig. 8. Streamlines and isolines for the longitudinal velocity (left) and the difference of normal components of the turbulent stress tensor (right) in the cross section $x = -0.25C$.
Calculations using *k*-*ω* SST (*a*), RSM-BSL (*b*), and BSL-EARSM (*c*) models.

velocity and prevents flow separation. The secondary flow can be reproduced both by differential (Fig. 8*b*) and algebraic (Fig. 8*c*) Reynolds stress models.

The pulsation of velocity components (i.e., Reynolds stress), being calculated using the RSM BSL model are in qualitative agreement with experimental data (Fig. 9). This graph shows that the Reynolds stress is close to zero in the free stream and starts increasing with the development of a boundary layer. The simulated pulsations for the longitudinal component of velocity are much lower than experimental data. However, the pulsations of wall-normal and the shear stress are in compliance with experiment. Experimental data on velocity pulsations (longitudinal and normal components) exhibit an additional maximum near the rear edge (not available in simulations). The shear stress at the vane tail changes the sign and this is explained by the recirculation zone.

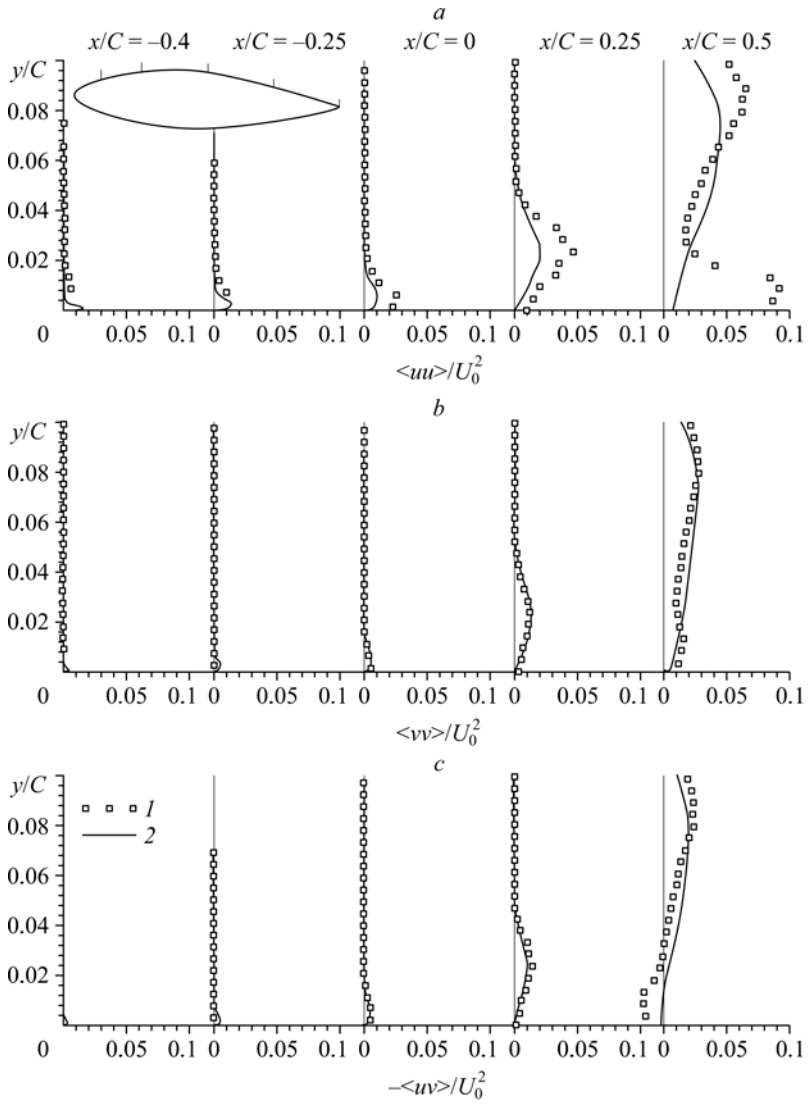

Fig. 9. Comparison of Reynolds stress using the RSM-BSL model with experimental data.
a — r.m.s for pulsations of longitudinal velocity,
b — r.m.s for normal velocity,
c — cross-correlation between the longitudinal and normal components of velocity (with opposite sign).

Conclusions

This study demonstrates that the modeling of turbulence is important in simulation of the finite-size hydrofoil. The significant 3D effects might take place, for example, for vanes in a hydroturbine, for stator column and the runner vanes. These cases cannot be limited by 2D simulations and require full 3D simulation. Meanwhile, the typical turbulence models (based on the linear turbulent viscosity approximation) are best tailored for simulation of planar shear flows and fail in describing the effects related to the anisotropy of turbulent pulsations.

For the considered case and for a flow past the vanes of a wicket gate (at rather high angle of attack), the k-ω SST model overestimates the separation zone sizes in the corner between the sidewall and the hydrofoil (this facilitates preventing the flow separation in the central plane). Both differential and algebraic RSM models can take into account the anisotropy of turbulent pulsations. Thus, it is capable to reproduce the secondary eddy flow in the corners; this flow transfers the momentum from the middle flow towards the sidewalls and this depresses the appearance of flow separation. As a result, the flow in the middle of channel becomes more two-dimensional and the flow separation occurs in the central plane.

The accuracy of CFD depends significantly on the grid resolution in the span direction and, mainly, on y_+ at the sidewall. If the values of y_+ are high, the RSM model at the sidewall gives the wrong estimations for flow separation in the central plane. Among these two considered Reynolds stress models, the best results were demonstrated by the RSM-BSL model that takes the turbulence dissipation rate equation from the k-ω baseline model, or the algebraic BSL-EARSM model with the same feature. Therefore, the accurate modeling of entire flow depends on several interdependent factors: flow separation for the vane, flow separation in the zone of hydrofoil-wall junction, and generated secondary flow.

References

1. **J. Nikuradse,** Untersuchungen über die Geschwindigkeits in turbulenten Strömungen, ForschHft. Ver. dt. Ing, Heft 281, 1926.
2. **E. Brundrett and W.D. Baines,** Production and diffusion of vorticity in duct flow, J. Fluid Mech., 1964, Vol. 19, P. 375–394.
3. **F.B. Gessner,** The origin of secondary flow in turbulent flow along a corner, J. Fluid Mech., 1973, Vol. 58, part 1, P. 1–25.
4. **P. Bradshaw,** Turbulent secondary flows, Annu. Rev. Fluid Mech., 1987, Vol. 19, P. 57–74.
5. **C. Speziale,** On nonlinear k-l and k-ε models of turbulence, J. Fluid Mech., 1987, Vol. 178, P. 459–475.
6. **B.A. Pettersson-Reif and H.I. Andersson,** Prediction of turbulence-generated secondary mean flow in a square duct, Flow, Turbulence and Combustion, 2002, Vol. 68, P. 41–61.
7. **A. Boudjir, T.J. Craft, and A. Turan,** Computational Investigation of flow through a rotating square duct by means of advanced second-moment closure, Flow, Turbulence and Combustion, 2007, Vol. 79, P. 99–122.
8. **G.A. Gerolymos and L. Vallet,** Reynolds-stress model prediction of 3Dd duct flows, Flow, Turbulence and Combustion, 2016, Vol. 96, P. 45–93.
9. **P. Orlandi, D. Modesti, and S. Pirozzoli,** DNS of turbulent flows in ducts with complex shape, Flow, Turbulence and Combustion, 2018, Vol. 100, P. 1063–1079.
10. **D. Von Terzi, H. Schneider, and H.-J. Bauer,** The impact of secondary mean vortices on turbulent separation in 3d diffusers, in: W.E. Nagel, D.B. Kröner, M.M. Resch (Eds.), High Performance Computing in Sci. and Engng, Springer-Verlag, Berlin, Heidelberg, 2011, P. 339–352.
11. **S. Parneix, P.A. Durbin, and M. Behnia,** Computation of 3-D turbulent boundary layers using the v2f model, Flow, Turbulence and Combustion, 1998, Vol. 60, P. 19–46.
12. **D.D. Apsley and M.A. Leschziner,** Investigation of advanced turbulence models for the flow in a generic wing-body junction, Flow, Turbulence and Combustion, 2001, Vol. 67, P. 25–55.
13. **R.B. Langtry, M. Kuntz, and F.R. Menter,** Drag prediction of engine-airframe interference effects with CFX-5, AIAA Paper, 2004, No. 2004-0391.
14. **2nd AIAA CFD** drag prediction workshop (DPW). Orlando, FL., June 21–22, 2003.
15. **F.R. Menter, A.V. Garbaruk, and Y. Egorov,** Explicit algebraic Reynolds stress models for anisotropic wall-bounded flows, Progress in Flight Physics, 2012, Vol. 3, P. 89–104.
16. **A.A. Gavrilov, A.V. Sentyabov, and K.A. Finnikov,** Numerical investigation of three-dimensional cavitating flow around a guide vane of a water turbine, Fluid Dynamics, 2019, Vol. 54, P. 441–450.
17. **M. Timoshevskiy, S. Churkin, A. Kravtsova, K. Pervunin, D. Markovich, and K. Hanjalic,** Cavitating flow around a scaled-down model of guide vanes of a high-pressure turbine, Intern. J. Multiphase Flow, 2016, Vol. 78, P. 75–87.

18. **A.V. Sentyabov, M.V. Timoshevskiy, and K.S. Pervunin,** Gap cavitation in the end clearance of a guide vane of a hydroturbine: numerical and experimental investigation, J. Engng Thermophys., 2019, Vol. 28, No. 1, P. 67–83.
19. **A.Yu. Kravtsova, D.M. Markovich, K.S. Pervunin, M.V. Timoshevskiy, and K. Hanjalic,** High-speed visualization and PIV measurements of cavitating flows around a semicircular leading-edge flat plate and NACA0015 hydrofoil, Int. J. Multiph. Flow, 2014, Vol. 60, P. 119–134.
20. **A.Yu. Kravtsova, D.M. Markovich, K.S. Pervunin, M.V. Timoshevskiy, and K. Hanjalic,** High-speed imaging of cavitation regimes on a round-leading-edge flat plate and NACA0015 hydrofoil, J. Visualization, 2013, Vol. 16, No. 3, P. 181–184.
21. **F.R. Menter,** Two-equation eddy-viscosity turbulence models for engineering applications, AIAA J., 1994, Vol. 32, No. 8, P. 1598–1605.
22. **D.C. Wilcox,** Turbulence modeling for CFD, Inc. La Canada, California: DCW Industries, 1998.
23. **B.E. Launder, G.J. Reece, and W. Rodi,** Progress in the development of a Reynolds-stress turbulence closure, J. Fluid Mech., 1975, Vol. 68, No. 3, P. 537–566.
24. **S. Patankar,** Numerical Heat Transfer and Fluid Flow, Hemisphere, N.Y., 1980.
25. **J.H. Ferziger and M. Peric,** Computational Methods for fluid dynamics. Springer-Verlag, Berlin, Heidelberg, 2002.
26. **B.P. Leonard,** The ULTIMATE conservative difference scheme applied to unsteady one-dimensional advection, Comp. Methods Appl. Mech. Engng, 1991, Vol. 88, P. 17–74.